REPORT DOCUMENTATION PAGE

Form Approved OMB NO. 0704-0188

1. REPORT DATE (DD-MM-YYYY)	2. REPORT TYPE	3. DATES COVERED (From - To)
05-01-2016	Final Report	1-Dec-2011 - 31-Oct-2016

4. TITLE AND SUBTITLE
Final Report: Capacitance-Voltage (CV) Measurement of Type-II Superlattice Photodiodes

5a. CONTRACT NUMBER
W911NF-12-2-0009

5b. GRANT NUMBER

5c. PROGRAM ELEMENT NUMBER
622712

6. AUTHORS
Manijeh Razeghi; Andy Chen

5d. PROJECT NUMBER

5e. TASK NUMBER

5f. WORK UNIT NUMBER

7. PERFORMING ORGANIZATION NAMES AND ADDRESSES
Northwestern University Evanston Campus
1801 Maple Avenue

Evanston, IL 60201 -3149

8. PERFORMING ORGANIZATION REPORT NUMBER

9. SPONSORING/MONITORING AGENCY NAME(S) AND ADDRESS (ES)
U.S. Army Research Office
P.O. Box 12211
Research Triangle Park, NC 27709-2211

10. SPONSOR/MONITOR'S ACRONYM(S)
ARO

11. SPONSOR/MONITOR'S REPORT NUMBER(S)
61310-EL.9

12. DISTRIBUTION AVAILIBILITY STATEMENT
Approved for Public Release; Distribution Unlimited

13. SUPPLEMENTARY NOTES
The views, opinions and/or findings contained in this report are those of the author(s) and should not contrued as an official Department of the Army position, policy or decision, unless so designated by other documentation.

14. ABSTRACT
This is the final report presents work progress of this project from December 1st, 2011 to February 29th, 2016. This work is aimed to achieve a comprehensive understanding of the dynamics of impurities in the InAs/GaSb Type-II superlattice (T2SL). Capacitance-voltage measurement has been performed to calculate the ionized reduced impurity concentration of the material. Measurements performed in a wide temperature range (7 K to 300 K) allow the extraction of activation energies and total concentrations of impurities. The evolution of the total impurity concentration and their activation energies has been modeled theoretically and compared with experimental

15. SUBJECT TERMS
Type-II, Superlattice, T2SL, Capacitance, CV

16. SECURITY CLASSIFICATION OF:			17. LIMITATION OF ABSTRACT	15. NUMBER OF PAGES	19a. NAME OF RESPONSIBLE PERSON
a. REPORT	b. ABSTRACT	c. THIS PAGE			Manijeh Razeghi
UU	UU	UU	UU		19b. TELEPHONE NUMBER 847-491-7251

Report Title

Final Report: Capacitance-Voltage (CV) Measurement of Type-II Superlattice Photodiodes

ABSTRACT

This is the final report presents work progress of this project from December 1st, 2011 to February 29th, 2016. This work is aimed to achieve a comprehensive understanding of the dynamics of impurities in the InAs/GaSb Type-II superlattice (T2SL). Capacitance-voltage measurement has been performed to calculate the ionized reduced impurity concentration of the material. Measurements performed in a wide temperature range (7 K to 300 K) allow the extraction of activation energies and total concentrations of impurities. The evolution of the total impurity concentration and their activation energies has been modeled theoretically and compared with experimental findings.
Ionized carrier concentration versus temperature dependence revealed the presence of a kind of defects with activation energy below 6meV and a total concentration of low 1015 cm-3. Correlation between defect characteristics and superlattice designs were studied. The defects exhibited a p-type behavior with decreasing activation energy as the InAs thickness increases from 7 to 11 monolayers, while maintaining the GaSb thickness of 7 monolayers. With 13 monolayers of InAs, the superlattice becomes n-type and the activation energy deviates from the p-type trend.
Capacitance-voltage technique was also utilized to characterize the carrier concentration of gallium-free InAs/InAs1-xSbx type-II superlattice p-i-n photodiodes as a function of growth temperature and Beryllium (Be) compensated doping. The unintentionally doped InAs/InAs0.45Sb0.55 superlattice photodiode grown at 395oC with 100% cut-off wavelength at 12 ?m has residually n-type carrier concentration of 1.6×10^15 cm^-3 at 77K. The background carrier concentration can be reduced by optimizing growth temperature and by Be-compensation doping. Different kinds of defects exist in the undoped InAs/InAs1-xSbx type-II superlattice and their dependence on the growth temperature was also investigated.

Enter List of papers submitted or published that acknowledge ARO support from the start of the project to the date of this printing. List the papers, including journal references, in the following categories:

(a) Papers published in peer-reviewed journals (N/A for none)

Received		Paper
08/31/2015	6.00	A. Haddadi, G. Chen, R. Chevallier, A. M. Hoang, M. Razeghi. InAs/InAsSb type-II superlattices for high performance long wavelength infrared detection, Applied Physics Letters, (09 2014): 1. doi: 10.1063/1.4896271
08/31/2015	8.00	A. Haddadi, R. Chevallier, G. Chen, A. M. Hoang, M. Razeghi. Bias-selectable dual-band mid-/long-wavelength infrared photodetectors based on InAs/InAs1?xSbx type-II superlattices, Applied Physics Letters, (01 2015): 1. doi: 10.1063/1.4905565
08/31/2015	7.00	Guanxi Chen, Abbas Haddadi, Anh-Minh Hoang, Romain Chevallier, Manijeh Razeghi. Demonstration of type-II superlattice MWIR minority carrier unipolar imager for high operation temperature application, Optics Letters, (12 2014): 1. doi: 10.1364/OL.40.000045
09/02/2014	5.00	M. Razeghi, A. Haddadi, A. M. Hoang, G. Chen, S. Bogdanov, S. R. Darvish, F. Callewaert, P. R. Bijjam, R. McClintock. Antimonide-Based Type II Superlattices: A Superior Candidate for the Third Generation of Infrared Imaging Systems, Journal of Electronic Materials, (03 2014): 0. doi: 10.1007/s11664-014-3080-y
09/30/2013	3.00	G. Chen, E. K. Huang, A. M. Hoang, S. Bogdanov, S. R. Darvish, M. Razeghi. Surface leakage investigation via gated type-II InAs/GaSb long-wavelength infrared photodetectors, Applied Physics Letters, (11 2012): 0. doi: 10.1063/1.4767905
09/30/2013	4.00	A. M. Hoang, S. Bogdanov, A. Haddadi, P. R. Bijjam, B.-M. Nguyen, M. Razeghi, G. Chen. Investigation of impurities in type-II InAs/GaSb superlattices via capacitance-voltage measurement, Applied Physics Letters, (07 2013): 0. doi: 10.1063/1.4813479
TOTAL:		**6**

Number of Papers published in peer-reviewed journals:

(b) Papers published in non-peer-reviewed journals (N/A for none)

Received		Paper
TOTAL:		

Number of Papers published in non peer-reviewed journals:

(c) Presentations

Number of Presentations: 0.00

Non Peer-Reviewed Conference Proceeding publications (other than abstracts):

Received	Paper

TOTAL:

Number of Non Peer-Reviewed Conference Proceeding publications (other than abstracts):

Peer-Reviewed Conference Proceeding publications (other than abstracts):

Received	Paper	
09/30/2013	2.00	A. M. Hoang, G. Chen, A. Haddadi, M. Razeghi, Manijeh Razeghi. High performance bias-selectable dual-band short-/mid-wavelength infrared photodetectors based on type-II InAs/GaSb/AlSb superlattices, SPIE OPTO. 05-FEB-13, San Francisco, California, USA. : ,

TOTAL: **1**

Number of Peer-Reviewed Conference Proceeding publications (other than abstracts):

(d) Manuscripts

Received	Paper

TOTAL:

Number of Manuscripts:

Books

Received Book

TOTAL:

Received Book Chapter

TOTAL:

Patents Submitted

Patents Awarded

Awards

Graduate Students

NAME	PERCENT_SUPPORTED	Discipline
Romain Chevallier	1.00	
FTE Equivalent:	**1.00**	
Total Number:	**1**	

Names of Post Doctorates

NAME	PERCENT_SUPPORTED
Sourav Adhikary	1.00
FTE Equivalent:	**1.00**
Total Number:	**1**

Names of Faculty Supported

NAME	PERCENT_SUPPORTED	National Academy Member
Manijeh Razeghi	0.02	
FTE Equivalent:	**0.02**	
Total Number:	**1**	

Names of Under Graduate students supported

NAME	PERCENT_SUPPORTED
FTE Equivalent:	
Total Number:	

Student Metrics

This section only applies to graduating undergraduates supported by this agreement in this reporting period

The number of undergraduates funded by this agreement who graduated during this period:	0.00
The number of undergraduates funded by this agreement who graduated during this period with a degree in science, mathematics, engineering, or technology fields:.....	0.00
The number of undergraduates funded by your agreement who graduated during this period and will continue to pursue a graduate or Ph.D. degree in science, mathematics, engineering, or technology fields:.....	0.00
Number of graduating undergraduates who achieved a 3.5 GPA to 4.0 (4.0 max scale):.....	0.00
Number of graduating undergraduates funded by a DoD funded Center of Excellence grant for Education, Research and Engineering:.....	0.00
The number of undergraduates funded by your agreement who graduated during this period and intend to work for the Department of Defense	0.00
The number of undergraduates funded by your agreement who graduated during this period and will receive scholarships or fellowships for further studies in science, mathematics, engineering or technology fields:	0.00

Names of Personnel receiving masters degrees

NAME
Total Number:

Names of personnel receiving PHDs

NAME
Total Number:

Names of other research staff

NAME	PERCENT_SUPPORTED
FTE Equivalent:	
Total Number:	

Sub Contractors (DD882)

Inventions (DD882)

Scientific Progress

See Attachment

Technology Transfer

Final Report

Capacitance-Voltage measurement of Type-II superlattice photodiodes (contract #W911NF-12-2-0009)

Report Dates Covered: **1 December 2011 – 29 February 2016**

Program Manager (COR): **Dr. William Clark, Tel: 919-549-4314**
william.w.clark@us.army.mil
william.w.clark9.civ@mail.mil

Principal Investigator: **Dr. Manijeh Razeghi**
razeghi@eecs.northwestern.edu
Northwestern University
Center for Quantum Devices
Cook Hall Room 4051
2220 Campus Drive
Evanston, IL 60208
Tel : 847-491-7251

Contents

Abstract:

This is the final report presents work progress of this project from December 1st, 2011 to February 29th, 2016. This work is aimed to achieve a comprehensive understanding of the dynamics of impurities in the InAs/GaSb Type-II superlattice (T2SL). Capacitance-voltage measurement has been performed to calculate the ionized reduced impurity concentration of the material. Measurements performed in a wide temperature range (7 K to 300 K) allow the extraction of activation energies and total concentrations of impurities. The evolution of the total impurity concentration and their activation energies has been modeled theoretically and compared with experimental findings.

Ionized carrier concentration versus temperature dependence revealed the presence of a kind of defects with activation energy below 6meV and a total concentration of low 10^{15} cm^{-3}. Correlation between defect characteristics and superlattice designs were studied. The defects exhibited a p-type behavior with decreasing activation energy as the InAs thickness increases from 7 to 11 monolayers, while maintaining the GaSb thickness of 7 monolayers. With 13 monolayers of InAs, the superlattice becomes n-type and the activation energy deviates from the p-type trend.

Capacitance-voltage technique was also utilized to characterize the carrier concentration of gallium-free InAs/$InAs_{1-x}Sb_x$ type-II superlattice *p-i-n* photodiodes as a function of growth temperature and Beryllium (Be) compensated doping. The unintentionally doped InAs/$InAs_{0.45}Sb_{0.55}$ superlattice photodiode grown at 395^{o}C with 100% cut-off wavelength at 12 μm has residually *n*-type carrier concentration of 1.6×10^{15} cm^{-3} at 77K. The background carrier concentration can be reduced by optimizing growth temperature and by Be-compensation doping. Different kinds of defects exist in the undoped InAs/$InAs_{1-x}Sb_x$ type-II superlattice and their dependence on the growth temperature was also investigated.

Key Words (Limit 5): CV measurement, homo-junction, Type-II superlattice, gallium-free

1. Background and Motivation

1.1. Development of Type-II superalttice

Type-II InAs/GaSb superlattices (T2SLs) were first proposed by Sai-Halasz *et al*[i]. in the 1970's. These superlattices are formed by alternating InAs and GaSb layers over several periods (Figure 1). This creates a one dimensional periodic structure, like that of the periodic atoms in naturally occurring crystals. InAs and GaSb are two members of the 6.1Å family which have a similar lattice constant around 6.1Å. This close lattice matching enables growth of T2SL with very high material quality.

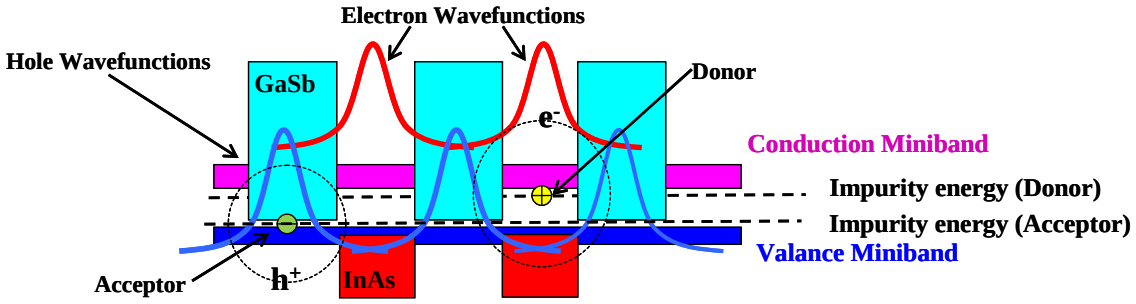

Figure 1: ***Spatial band alignment in Type-II superlattice (red regions represent InAs forbidden gap and cyan regions represent GaSb forbidden gap)***

More importantly, the Type-II band alignment of the material (configuration in such the conduction band of InAs lies below the valence of GaSb (Figure 1) causes the separation of electrons and holes into the InAs and GaSb layers, respectively. This charge transfer gives rise to a high local electric field and strong interlayer tunneling of carriers without the requirement of an external bias or additional doping. The resulting energy gap depends upon the layer thicknesses and interface compositions. In reciprocal space, the system is a direct-bandgap material with a high transition probability and a high optical absorption coefficient. This makes Type-II superlattices an attractive approach for realizing infrared photodetectors.[ii]

In recent years, T2SL has experienced a drastic development, attaining a performance level comparable to state of the art MCT detectors.[iii] Major advances in detector performance have enabled the demonstration of infrared focal plane arrays (FPAs) with excellent quality. However, these achievements to date only take advantage of the band gap tunability of T2SL, whereas this is a quantum mechanical material system and still offers quantum mechanical advantages that haven't yet been fully explored and utilized. For example, Auger recombination, which is a limiting factor for high temperature operation of infrared detectors, can be suppressed by manipulating the superlattice to control the band structure. Compared to MCT and most other small band gap semiconductors that have very small electron and hole effective masses, the effective masses in T2SLs are relatively large, due to its superlattice design which involves the interaction of electrons and holes via tunneling through adjacent barriers. By adjusting the

superlattice design the effective masses can be increased further to reduce the tunneling current, which is a major component of the dark current in MCT detectors. Moreover, the capability of band structure engineering opens the horizon for exploring novel device architectures that are unthinkable using simple binary or ternary compound semiconductor band alignments like MCT. Recent research has proposed a novel variant of T2SL, the M-structure SL, with large effective mass and large tunability of band edge energies.

Despite these attractive promises, there is still a large gap between the theoretical capabilities of this material system and the experimental performance of T2SL based detectors. This is partially because of the presence of impurities and imperfection in the material. Each Type-II structure consists of hundreds of alternating layers, each only a few mono-layers thick. Crystallographically stacking so many layers, along with the thousands of mechanical MBE shutter actuations required to physically grow the layers, introduces diverse imperfections in the material. These impurities disrupt the atomic periodic potential, disturbing the bandstructure, creating scattering centers, thus leading to deterioration of material quality evidenced by degradation of the carrier lifetime and mobility. Understanding the physics of impurities in T2SL is critical to achieve high performance devices.

This work will aim to characterize the concentration and ionization activation energy of impurities in T2SL via Capacitance-Voltage (CV) measurement. Knowing the background impurity concentration and activation energy, and their evolution with temperature and different superlattice configurations will offer novel strategies to mitigate negative effects of impurities in T2SL materials. Superlattices can be designed with higher purity, longer carrier lifetimes, and thus enabling further improvement of device performance.

In recent years, the limiting factors are being attributed to the surface leakage problem and the short carrier lifetime due to Shockley-Read-Hall (SRH) centers[iv]. While different surface treatment techniques have been proposed[v,vi,vii] to solve the surface leakage problem, suppressing the SRH process is the key to achieve the theoretically predicted bulk performance. Since native defects in the GaSb are responsible for the SRH process, InAs/$InAs_{1-x}Sb_x$ system is proposed and predicted to have longer carrier lifetimes, which results in lower dark current[viii,ix,x,xi,xii].

Since InAs and $InAs_{1-x}Sb_x$ materials are both residually *n*-type, the unintentionally doped InAs/$InAs_{1-x}Sb_x$ superlattices (SLs) is expected to be *n*-type[xiii,xiv,xv,xvi]. The reported residual carrier concentration of mid-wavelength infrared (MWIR) unintentionally doped InAs/$InAs_{1-x}Sb_x$ SLs is ~ 2×10^{16} cm^{-3} at 10K[xvii], which is two orders of magnitude higher than the one reported in InAs/GaSb T2SL[xviii] system. Since the residual background carrier concentration determines the minority carrier concentration and minority carrier lifetime, which is strongly related to the detector's electrical and optical performance, with such high residual background carrier concentration, it is very difficult to achieve low dark current and high quantum efficiency photodetector. Therefore, understanding what kinds of impurities exist in the InAs/$InAs_{1-x}Sb_x$ SLs and finding a method to achieve high purity InAs/$InAs_{1-x}Sb_x$ SLs are crucial for high performance detector. In this part of the project, we utilized temperature dependent capacitance-voltage measurement to investigate the background carrier concentrations as a function of

growth temperature and subsequently, its dependence on Beryllium (Be) compensated doping level in the long-wavelength infrared (LWIR) InAs/$InAs_{1-x}Sb_x$ T2SLs photodetectors.

1.2. Theory of C-V Measurement

1.2.1. Impurities in Semiconductors and Low Dimensional Systems

Real semiconductor material is never perfect. Even when it is not intentionally doped, imperfections arise due to impurities or a perturbation of the periodical crystalline structure. They can act as either a deep center or a shallow center, depending on their energy level with respect to the valence band and the band gap of the material. Shallow impurities produce the most noticeable effects on the material quality as they are closer to the band edge. They can be either donors or acceptors, which can provide mobile charges via thermal ionization:

$$N^{ionized} = N^{Total} \exp\left(-\frac{E_a}{k_B T}\right) \qquad (1)$$

N^{total} : total concentration of defects (acceptor or donor)

$N^{ionized}$: thermally ionized concentration of defects

E_a : the activation energy

k_B : the Boltzmann constant

T : the absolute temperature

At low temperature, mobile carriers generated by the generation process dominates over thermally generated carrier, the total mobile carrier concentration equals the ionized impurity concentration. In such case, the semiconductor is under extrinsic regime, and the dynamic of mobile carriers depends on the ionization processes.

Impurities and ionization processes are well-known in bulk semiconductors. By using the hydrogen atom model, the activation energy can be estimated as a function of carrier effective mass m^* and material permittivity ε

$$E_a = \frac{q^4 m*}{2(4\pi\varepsilon\varepsilon_0)^2\hbar^2} \qquad (2)$$

and the Bohr radius R_i of the hydrogen-atom-like impurities is

$$R_i = \frac{4\pi\varepsilon\varepsilon_0\hbar^2}{m*q^2} \qquad (3)$$

$\hbar$ is the Plank's constant,

ε_0 is the vacuum permittivity

ε is the material relative permittivity

q is electron charge

In a low dimensional system, for example a quantum well, the activation energy is affected when the well width tends to be comparable to the Bohr radius. Quantum mechanical confinement reduces the "mobility" of the carriers, making the activation energy increase when the confinement effect is stronger. This phenomenon has been well-studied and verified experimentally for various quantum well systems. However, in a superlattice system where multiple quantum wells are put close to each other and the interaction between adjacent wells are non negligible, the quantum processes become more complicated and are not well understood. The well width in a superlattice is normally on the order of tens of Angstroms, which is well below the Bohr radius of impurities (typically ~100 Å with an activation energy below 10 meV for low bandgap materials). The effect of quantum confinement will be stronger and more significant than in the case of quantum wells. Besides quantum confinement of carriers in potential wells, the tunneling and interaction of carriers in different quantum wells become non-negligible factors. This additional degree of freedom is expected to reduce the effects of quantum confinement, and weaken the variation of activation energy on the layer thickness.

1.2.2. Carrier Concentration and Activation Energy Determination

Capacitance-voltage measurement is performed on a p-n junction under applied reverse biased to extract the reduced concentration. Mobile charges (electrons and holes) are completely swept out of the depletion region, leaving fixed ionized impurities (donor-like and/or acceptor-like). These space charges act as a capacitor with capacitance C, depletion width W_d, and reduced concentration are:

$$C = \frac{\varepsilon \varepsilon_0 A}{W_d} \tag{4}$$

$$W_d = \sqrt{\frac{2\varepsilon\varepsilon_0}{q}\left(\frac{1}{N_a^{ionized}} + \frac{1}{N_d^{ionized}}\right)(V_{bi} + V)} \tag{5}$$

$$N_{reduced} = \frac{1}{1/N_a^{ionized} + 1/N_d^{ionized}} = \frac{2}{q\varepsilon_{SL}\varepsilon_o \dfrac{d(A^2/C^2)}{dV}} \tag{6}$$

ε_0 is the vacuum permittivity ε is the material relative permittivity

$N^{ionized}_{a,d}$ are the ionized acceptor and donor concentrations q is electron charge

V_{bi} and V are the built in and applied voltages A is the junction area

2. Work completed

2.1. Measurement System Improvement

The C-V measurement system consists of a Janis STVP-100 two chamber liquid helium optical cryostat with 34-feed-throughs, a Keithley 707A 6-slot switching matrix with five model 7174A low-current and high-speed matrix cards, and a four terminals HP 4192A low-frequency impedance analyzer (LFIA). Since there are a lot of long cables (4 coaxial cables, 34 one meter long triaxial cables between the switching matrix and cryostat, and 34 wires inside the cryostat) between the terminals of LFIA and the samples (Figure 2), all those cables must be characterized to have the same impedance for high accuracy requirement. If all those cables does not have the same impedance, open circuit and shot circuit calibration will not work, which is the requirement before performing the C-V measurement.

In order to improve the accuracy of measurement, I replaced the wires inside the cryostat with high quality, low impedance stranded copper wires, which can be used from <1 K to 400K. Compare the leakage current level before and after rewiring, the leakage current level of the system is at 10^{-7} A/cm^2 before, but it reduces to 10^{-9} A/cm^2 level, which it's a 2 order of magnitudes reduction (Figure 3). More importantly, all 32 pins have the same level of leakage current, which means all 32 wires have the same impedance.

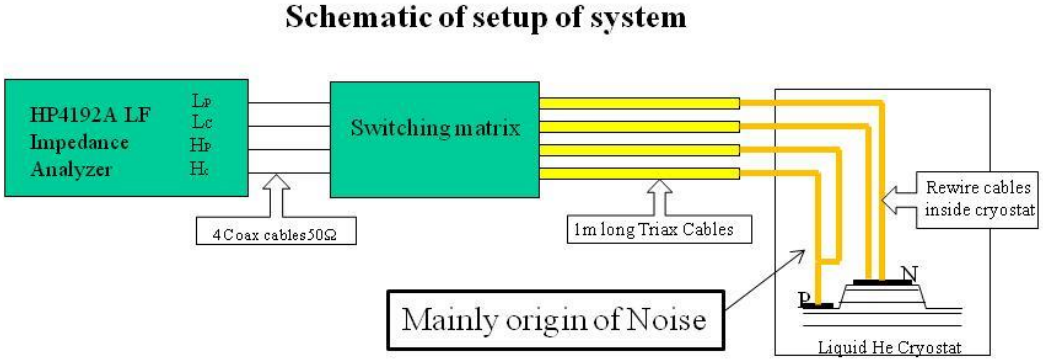

Figure 2: ***The schematic of the CV measurement system, including low-frequency impedance analyzer, switching matrix, liquid He cryostat and all cables.***

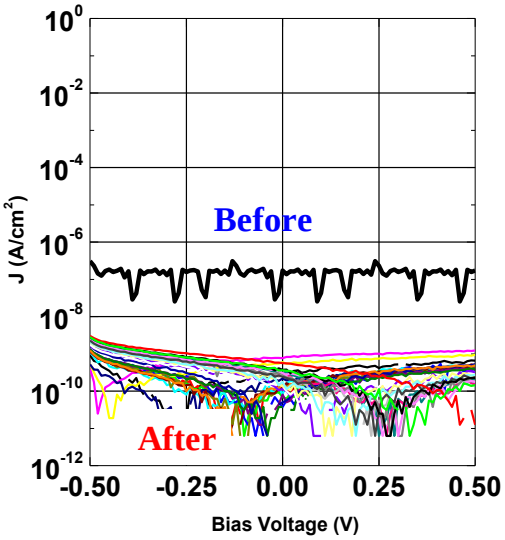

Figure 3: ***Leakage current level of the system before and after re-wiring. After wiring, the leakage current levels of all 32 pins were tested.***

2.2. Design and Material Growth

All four designs, denoted A, B, C, and D consisting of 7 monolayers (ML) of GaSb, and 7, 9, 11, and 13 MLs of InAs respectively, were grown (Figure 4). The band gaps calculated by ETBM for all samples are 252 meV, 194 meV, 149meV, and 114meV, respectively (Table 1). These four samples were all grown on GaSb (001) n-doped wafers by Intevac Modular Gen II molecular beam epitaxy system equipped with As/Sb valved cracker cells and Ga/In SUMO® cells. They all have the same device structures, consisting of a 0.5 μm thick GaSb:Be p^+ buffer, a 0.5μm InAs/GaSb:Be p^+ region, a 2μm nid InAs/GaSb active region, a 0.5μm InAs:Si/GaSb n^+ region, and a 10 nm InAs:Si n^+ doped top contact layer. Material characterization with high resolution x-ray diffraction shows consistent SL periods with the theoretical values.

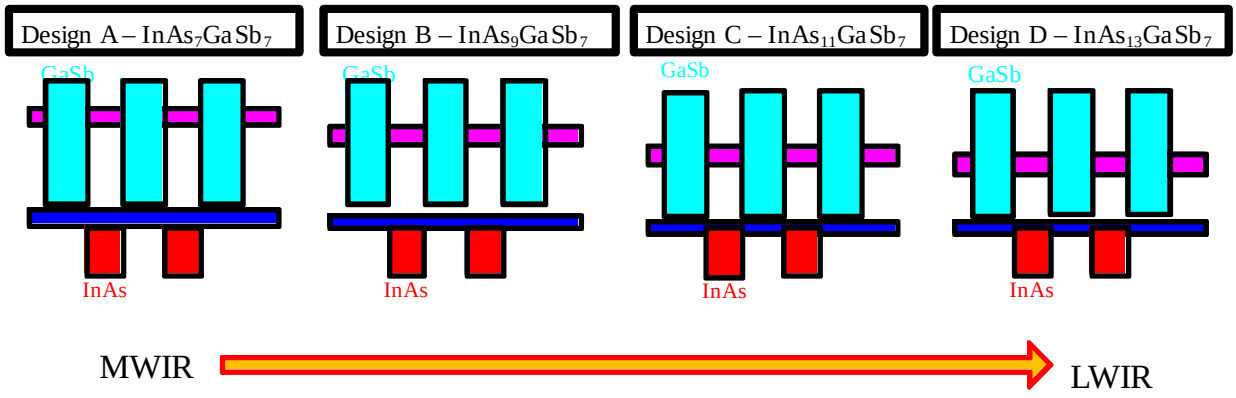

Figure 4: ***Designs of four samples with different superlattice designs***

2.3. Optical Characterization

All samples were processed by using standard processing technique[xix]**Error! Reference source not found.**. They were not passivated but were kept in vacuum chamber to minimize the exposure to ambient atmospheric conditions. All samples were measured in the Janis Liquid Helium cryostat at 77K by exactly the same way. The optical characteristics of all samples were first measured in a Janis Liquid Helium cryostat at 77K. The analysis of each sample was performed on sets of diodes with sizes from 100 x 100 μm to 400 x 400 μm.

The quantum efficiency (QE) versus wavelength of each sample, the QE at peak responsivity, 50% cut-off wavelength, the calculated band gap based on the empirical tight binding model (ETMB)[xx], and the measured band gap determined from the QE measurement of each sample are shown on Figure 5, Figure 6, and Table 1. The bandgap extracted from QE measurement and ETBM theoretical calculation is well matched (Table 1). The QE of sample B is similar as sample A. Since InAs is natively n-type and GaSb is natively p-type, the undoped superlattice can be either p-type or n-type depending on the thickness ratio between InAs and GaSb. Thicker InAs tends to result in n-type materials whereas thinner InAs would make p-type materials. Sample A, B, and C have similar levels of QE despite different cut-off wavelengths, but sample D exhibits a significantly lower value. The discrepancy of the QE between sample D and the first three samples is due to different types of residual background of superlattice. Indeed, thicker InAs tends to result in n-type material whereas thinner InAs would make the material p-type. Minority electrons have longer diffusion length than minority holes which results in higher QE of p-type material[xxi]. Since the nid 13 MLs InAs/7 MLs GaSb design have been proven to exhibit n-type semiconductor characteristic[xxii], we can conclude that sample A, B, and C have residually p-type background, and sample D is n-type. This remark provides useful

information for the C-V measurements since the C-V technique is incapable to determine the charge sign of carriers.

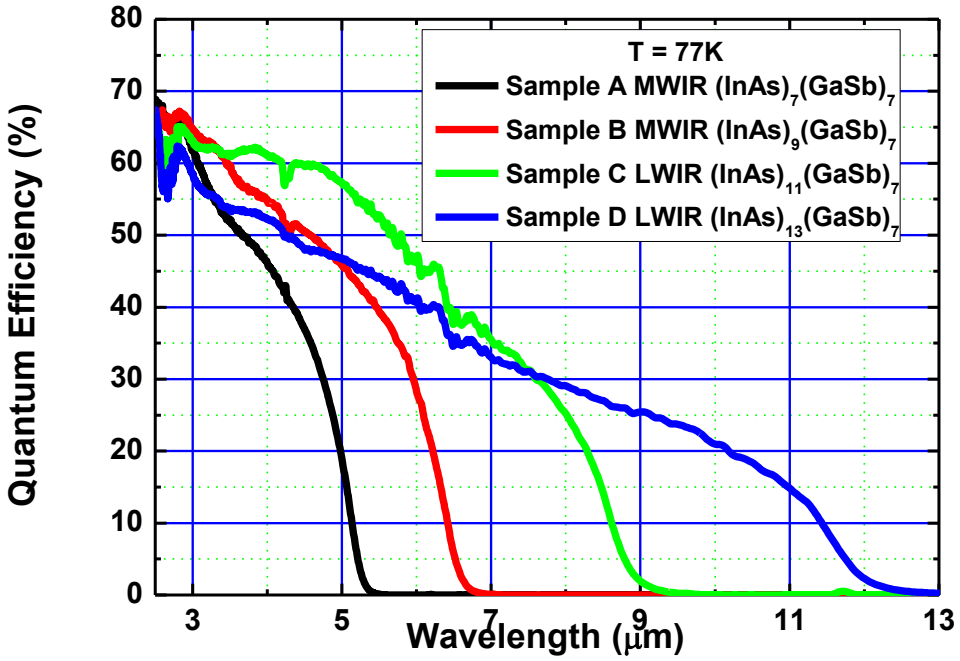

Figure 5: The quantum efficiency of sample A and B at peak responsivity.

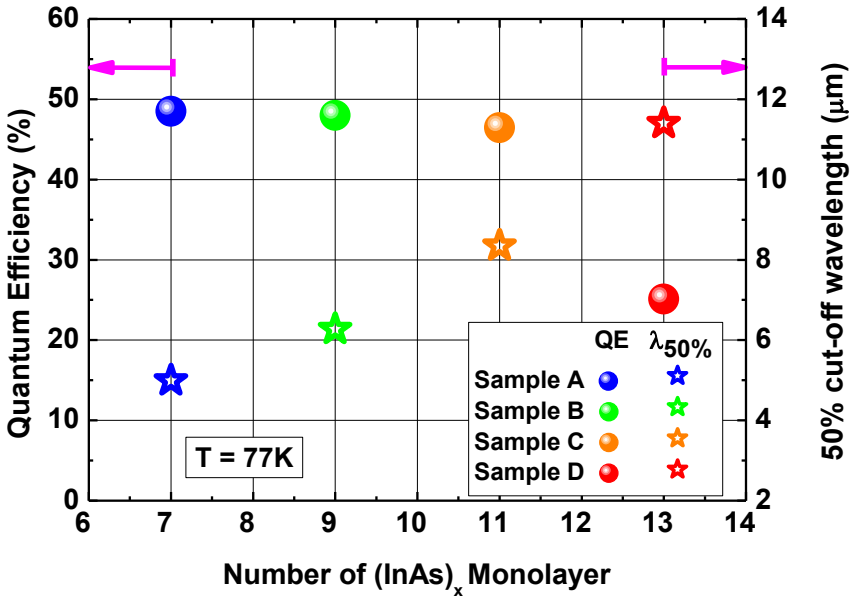

Figure 6: The quantum efficiency at peak responsivity and 50% cut-off wavelength of different designs at 77K

2.4. C-V measurement

After the optical measurement, four best diodes with sizes from 250 × 250 μm to 400 × 400 μm from each sample were chosen for C-V measurement at temperatures ranging from 7K to 120K achieved by liquid helium cooling. The reduced carrier concentration can be extracted from the slope of the linear fitting curve to the square of A/C versus the reverse bias voltage as explained by equation (6), where A is the diode area, C is the capacitance, V is the applied bias on the diode, q is the electron charge, and ε_o is the vacuum permittivity. Regardless of the residual carrier type in the nid region, the junction is heavily asymmetric due to the highly doped p+ and n+ contacts sandwiching the nid region (p+n for intrinsically n-type nid region, or n+p for intrinsically p-type nid region), the measured reduced concentration is the ionized carrier concentration in the nid region. For relative permittivity, ε_r, we choose 15.4, a value between InAs and GaSb. Figure 7 shows the reduced carrier concentration at temperature between 7K and 120K for a set of four diodes from each sample. The error bar for each data point was estimated from the error of the linear fit of the $(A/C)^2$ vs V slope.

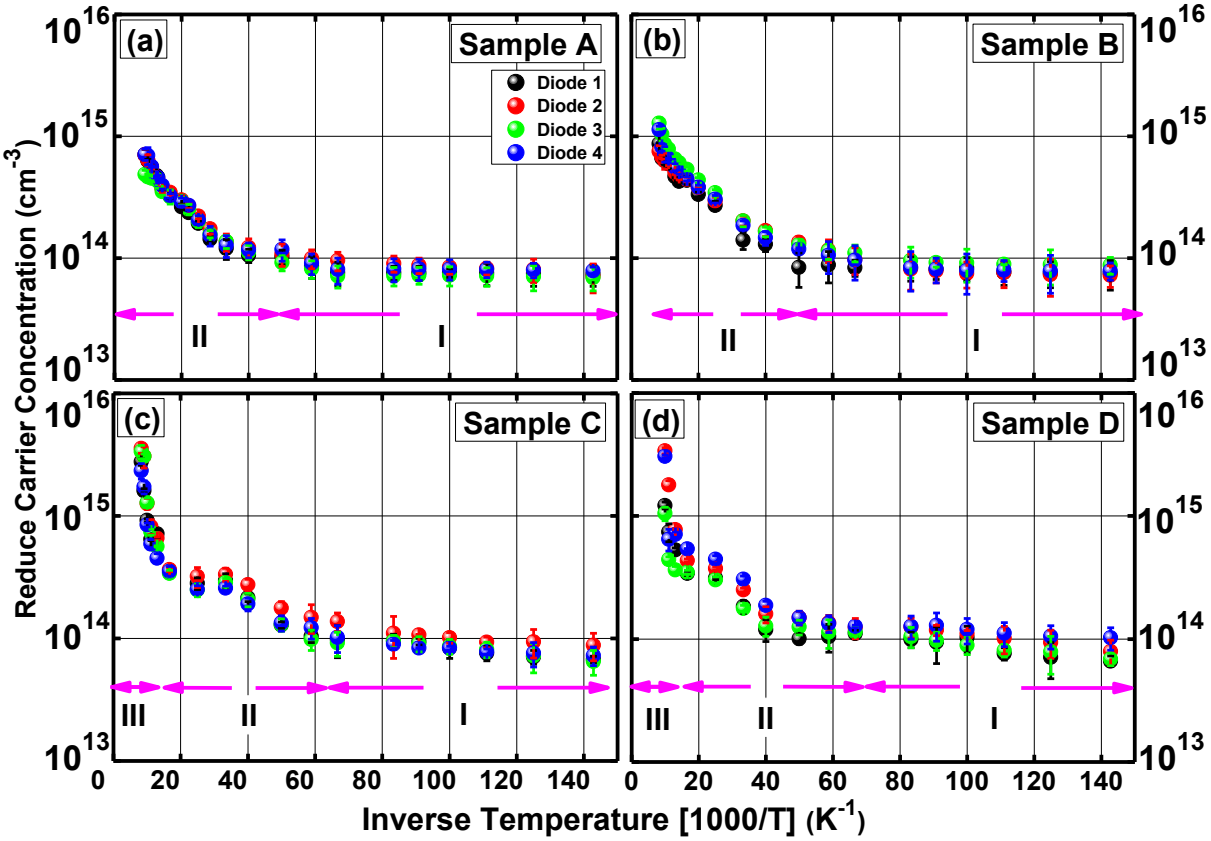

Figure 7 ***The reduce carrier concentration versus inverse temperature of sample A with $(InAs)_7(GaSb)_7$***

The temperature dependence of the reduced carrier concentration can be subdivided into three regions. Region I refers to the 1st kind of shallow level defects saturation regime. These defects have very small activation energy and are completely ionized even at very low temperature. Region II corresponds to the extrinsic region of the 2nd kind of shallow level defects. Regime III corresponds to the intrinsic regime. At low temperature, all samples stay in the Region I (7K to 20K for sample A and B, and 7K to 15K for sample C and D), and their background concentrations do not change with temperature, which corresponds to the saturation a type of shallow defects. This type of defects has a concentration around 1×10^{14} cm^{-3} and activation energies well below the thermal energy at 7K (0.6 meV). It is worth noting here that carefully analysis has been done to verify that the low constant concentration is not due to the limit of the system. At higher temperature, all four samples get into the Region II (20K for sample A and B, and 15K sample C and D) and their concentrations vary exponentially with the inverse temperature. The activation energies extracted from the slope of Region II of all four samples are reported in Table 1. The extrinsic region of sample A and B extends up to 120K and the intrinsic region is only observed in sample C and D. That is because sample C and D have relatively smaller band gap than sample A and B.

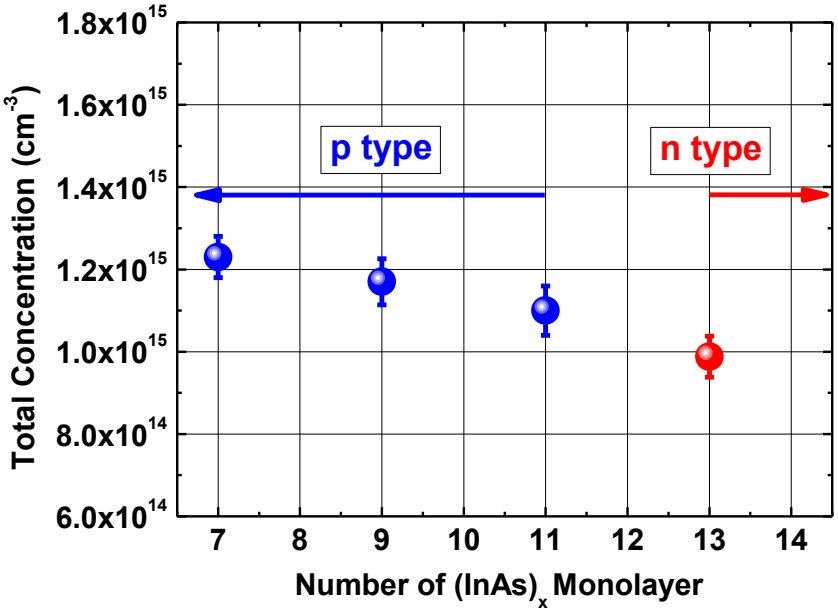

Figure 8 ***The reduce carrier concentration versus inverse temperature of sample B with $(InAs)_9(GaSb)_7$***

The total concentration of 2nd kind of shallow level defect (N_{Total}) can be extracted from equation (1). The values of N_{Total} of each sample are shown in Table 1 and Figure 8. This weak decrease of total concentration with the increase of InAs monolayer is due to the compensation of natively p-type GaSb by the n-type InAs of increasing thickness. Once the InAs layer is thick enough, type inversion happens. However, one should not expect the carrier concentration by the weight average of the donor and acceptor charges in the InAs and GaSb layer respectively because of the complicated convolution with the design-dependent activation energy as discussed below.

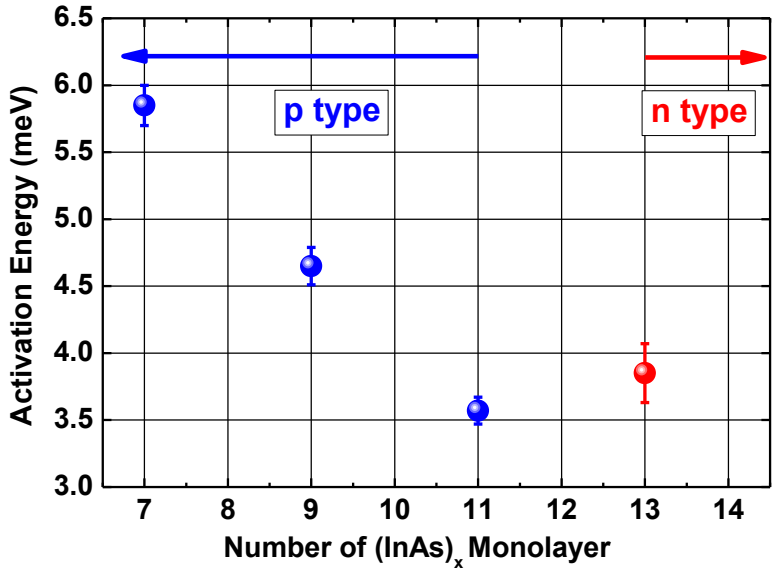

Figure 9 ***The reduce carrier concentration versus inverse temperature of sample C with*** $(InAs)_{11}(GaSb)_7$

As shown in Figure 9, the activation energy of the 2nd kind of defect decreases as the InAs ML increases from 7 to 11 and then deviates from the trend at InAs ML = 13. This deviation could again be the result of background type inversion between samples D and the others. In the multiple-quantum well system, which is the case of type-II superlattice, the behavior of activation energy of impurity depends on the quantum well width, barrier width and the barrier height. As the barrier width increases, wave function is forced to localize around the impurity ion because the penetration of wave function itself through the barrier becomes harder. This localization effect tends to increase the activation energy. One the other hand, the thickness of the barrier in the superlattice is in the range that the wave functions penetration from adjacent wells cannot be neglected; these penetrated wave functions repulse each other, and thus increase the localization of the wave function around the impurity ion. However, increasing the thickness of barrier weakens this repulsive effect, which causes the wave function delocalization and results in the reduction of the activation energy. The behavior of activation energy depends on the strength of these two completing effects. In the case of superlattice, the competition is expected to be more complicated due to the thin constituent layers and strong tunneling via the broken band gaps. However, experimental results suggest that the delocalization effect is stronger than the localization effect from the increment of the barrier and leads to the reduction of activation energy.

Table 1: Summary of Design Characteristics

	Smaple A	Sample B	Sample C	Sample D
Design	$(InAs)_7(GaSb)_7$	$(InAs)_9(GaSb)_7$	$(InAs)_{11}(GaSb)_7$	$(InAs)_{13}(GaSb)_7$
Mismatch (ppm)	4017	2370	1025	-84
$\lambda_{50\%}$ (μm)	5.00	6.26	8.35	11.4
QE (%) at peak responsivity	48.5	48.0	46.5	25.2
$E_{g\text{-}ETBM}$ (meV)	252	194	149	114
$E_{g\text{-}QE}$ (meV)	248.6	187.8	148.5	109.3
E_a (meV)	5.85 ± 0.15	4.52 ± 0.12	3.57 ± 0.10	3.85 ± 0.22
N_{Total} (cm^{-3})	$(1.23\pm0.09)\times10^{15}$	$(1.17\pm0.1)\times10^{15}$	$(1.10\pm0.15)\times10^{15}$	$(9.88\pm0.8)\times10^{14}$

2.5. Design and Material Growth of LWIR InAs/InAs$_{1-x}$Sb$_x$ materials

For this study, all different LWIR InAs/$InAs_{1-x}Sb_x$ materials were grown on an *n*-type GaSb substrate with molecular beam epitaxy and differed by their growth temperature and active region doping level. Shown in Figure 10 is the device structure used for the C-V measurement. The structure consists of a 0.1 μm-thick GaSb buffer layer, following by a 0.5 μm-thick n^+-doped $InAs_{0.91}Sb_{0.09}$ etch stop layer and a 3 μm-thick *n-i-p* T2SL photodiode structure. Finally, it was capped with 20 nm-thick p^+-doped InAs capping layer. The device contained 0.5 μm-thick Silicon doped n^+-contact ($n^+\sim10^{18}$ cm^{-3}), 2 μm-thick active region, and 0.5 μm-thick Be-doped p^+-contact ($p^+\sim10^{18}$ cm^{-3}). The superlattice design contains 28/7 mono-layers (MLs) of InAs/$InAs_{0.45}Sb_{0.55}$ in one period. All materials were processed by the same processing technique as reported in Ref. vii. After processing, all samples were kept unpassivated, wire-bonded onto a 68 pin leadless chip carrier, and loaded into a cryostat for characterizations. Five diodes with

sizes ranging from 250×250 μm to 400×400 μm from each sample were chosen for C-V measurement. The C-V measurement technique is described in detail previously[xxiii].

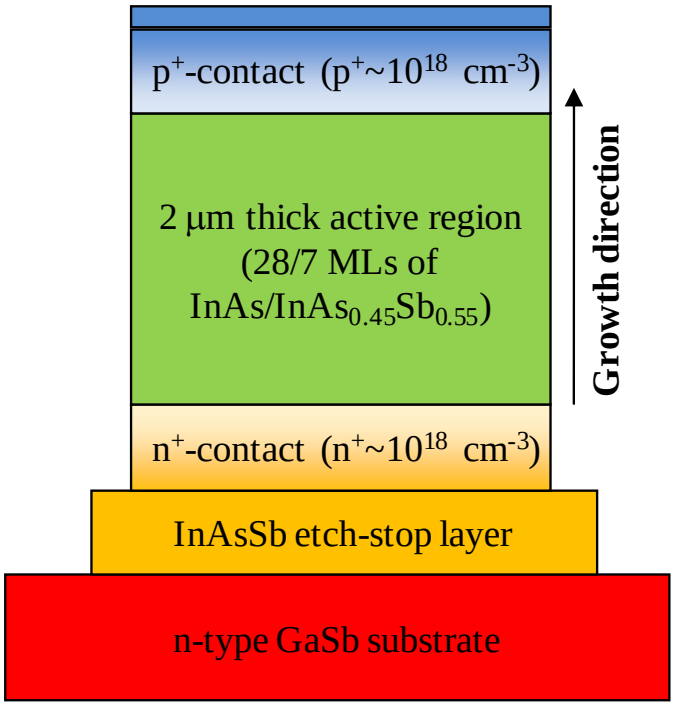

Figure 10: ***Schematic diagram of device structure used for C-V measurement***

2.6. C-V measurement of LWIR InAs/InAs$_{1-x}$Sb$_x$ materials

In the first stage of this study, we investigated the influence of the growth temperature on carrier concentration in the InAs/InAs$_{0.45}$Sb$_{0.55}$ superlattices for LWIR materials. Samples with active region intentionally undoped were grown at three different growth temperatures (T_G) 385, 395 and 405^{o}C.

At 385^{o}C, the epitaxy growth was not at optimal condition which resulted in low quality of crystallinity that was confirmed by Atomic Force Microscopy (AFM) and high resolution X-ray diffraction (HR-XRD). The device processed from this material exhibited poor electrical and optical performance. Therefore, it was not good enough to be utilized in C-V measurement technique. At 395 and 405^{o}C, although structural characterizations of the grown materials exhibited standard crystallinity, the background carrier concentration exhibited a large discrepancy. Shown in Figure 11 is the carrier concentration evolutions as function of temperature of samples grown at 395^{o}C (sample A_0) and at 405^{o}C (sample B_0).

From their similar pattern of the illustrated evolutions of defect levels with temperature, two different kinds of defects are observed. Indeed, the temperature dependence of the reduced carrier concentration can be subdivided into four regions. Region I corresponds to the intrinsic regime. Region II and III refers to the saturation region and the extrinsic region of the deep level defects. Region IV corresponds to the saturation region of a shallow level defect.

On the one hand, it can be seen that for temperatures above 35 K when the defects of deep level get ionized, the sample A_0 grown at low temperature (at 395°C) consistently achieved a lower background carrier concentration than the one grown at 405°C. At 77 K, the reduced carrier concentration of sample A_0 reached the value of 1.6×10^{15} cm^{-3}. This result is comparable to the one reported for the InAs/GaSb SLs and much lower than the previously reported results of InAs/$InAs_{1-x}Sb_x$ grown and measured by other groups.

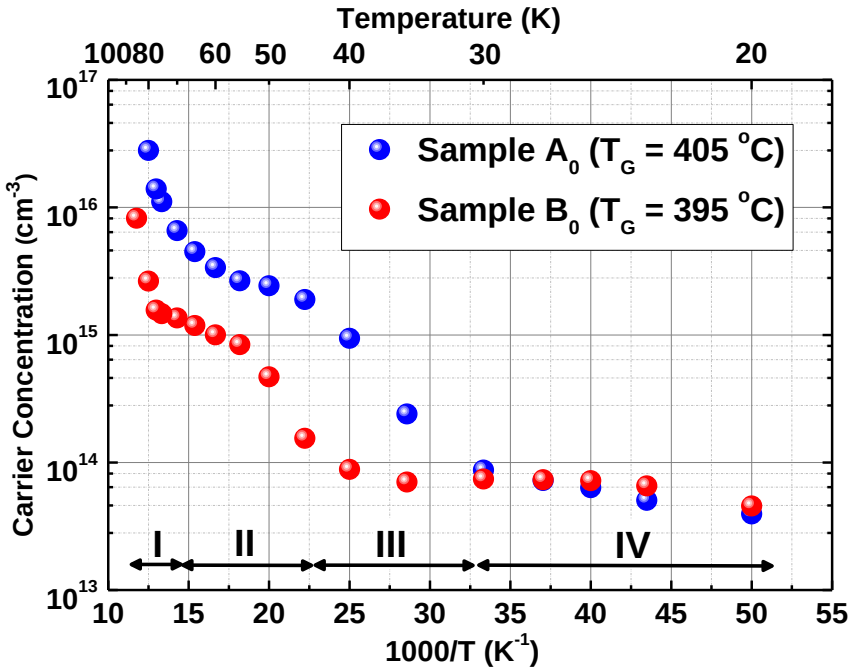

Figure 11: ***Comparison of the evolution of reduced carrier concentration with temperature between sample A_0 and B_0. Sample A_0 is grown at 405 °C and Sample B_0 is grown at 395°C.***

On the other hand, at low temperature (<30K) the reduced carrier concentrations of both samples saturate at the same level (~7×10^{13} cm^{-3}). This indicates that growth temperature do not have much effect on the shallow level defects. Even though the influence of the growth temperature on the carrier concentration is clearly proved, the type and origin of the defects are still unclear at this moment and need further investigation.

In the second stage of this study, we attempted to further understand the defects of this material. InAs and $InAs_{1-x}Sb_x$ are well-known to be natively *n*-type, as a consequence, it follows that the InAs/$InAs_{1-x}Sb_x$ type-II superlattices are also of intrinsically *n*-type material. In order to achieve a low carrier concentration or intentionally *p*-dope this material, the introduction of Beryllium has been chosen as a compensated doping[xxiv] (As can be seen later).

For this study, four more samples with active region doped with Beryllium with doping level of 6×10^{15}, 2×10^{16}, 3×10^{16}, 5×10^{16} cm^{-3} and denoted as B_1, B_2, B_3 and B_4, respectively were grown consecutively. We chose to grow the structures at 405°C since at this temperature, the defects are more present and the effect would be more profound and more observable. Shown in

Table **II** is the summary of all the samples used in this study with the carrier concentrations C-V measurement performed at 77K. Figure 12**:** shows the carrier concentration of the samples B_0 to B_4.

Sample	A	B_0	B_1	B_2	B_3	B_4
Growth Temperature (°C)	395	405	405	405	405	405
Doping Level (cm^{-3})	NA	NA	6×10^{15}	2×10^{16}	3×10^{16}	5×10^{16}
Carrier Concentration at 77K (cm^{-3})	1.6×10^{15}	1.2×10^{16}	5.7×10^{15}	9.7×10^{15}	1.5×10^{16}	3.7×10^{16}

Table II: ***Growth temperature, doping level and carrier concentration at 77K for sample A, B_1, B_2, B_3 and B_4.***

At 77K, the background carrier concentration of the intentionally undoped sample (B_0) is 1.2×10^{16} cm^{-3}. As can be seen, with the presence of Beryllium, the reduced carrier concentration starts decreasing, which is an indication of the Be-compensation effect for the n-type defects of the material. Sample B_1 with Be-doping level of 6×10^{15} cm^{-3} exhibits the lowest carrier concentration, with value of 5.7×10^{15} cm^{-3}, which is 2.1 times lower than Sample B_0. At Be doping level of 1.5×10^{16} cm^{-3} (Sample B_2), the reduced carrier concentration starts increasing, which suggests that the SLs already changes from *n*-type to *p*-type and the dominant defects are caused by the external doping of Be. As the Be-doping level increases, the reduced carrier concentration keeps on increasing (Sample B_3 and B_4).

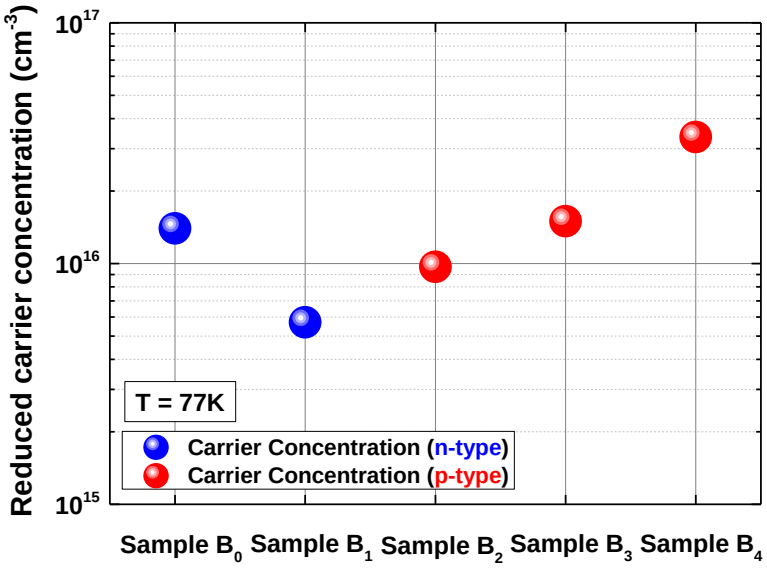

Figure 12: ***Influence of Be-doping on the carrier concentration of LWIR InAs/InAs$_{1-x}$Sb$_x$ SLs.***

In order to study the effect of Be-doping on different kinds of defects, C-V measurement was performed for intentionally undoped sample (B_0) and doped sample (B_1) on a large range of measuring temperature from 20K to 85K (Figure 13). The reduced carrier concentration of Sample B_1 is lower than the undoped one in the whole temperature range, which means that Beryllium compensates both deep and shallow level defects. However, even though with lower carrier concentration, sample B_1 exhibits similar evolution with temperature as the sample B_0 for most of the regimes (region I, II and III) and only differs significantly at region IV (at very low temperature < 30K). While in undoped sample, region IV_A corresponds to the saturation region of a shallow level defect (Sample B_0), in the Be-doped sample, region IV_B corresponds to the extrinsic region of the Be (Sample B1).

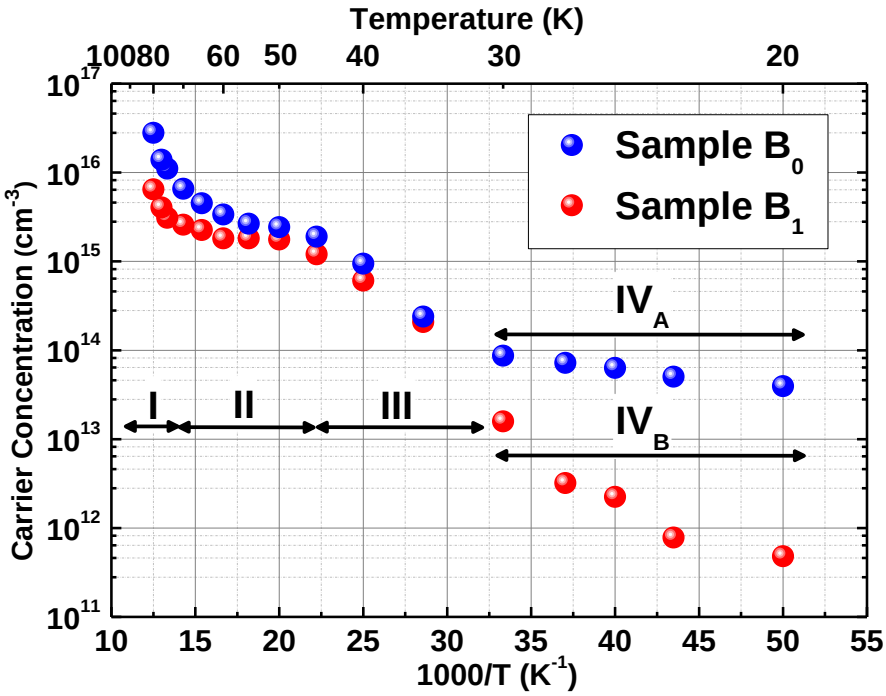

Figure 13: ***Comparison of the evolution of reduced carrier concentration with temperature between sample B_0 and B_1. Sample B_0 is intentionally undoped and Sample B_1 is doped with Be.***

Since the electrical and optical performance of unintentional doped *p-i-n* photodiode with low background carrier concentration is important, in the next part, we report the electrical and optical characteristics of sample A which is grown at 395°C and achieves lowest carrier concentration

Figure 14(a) shows the electrical characteristic of Sample A at different temperatures from 25K to 77K. At 77K, the dark current density at -50mV (J_{-50mV}) and differential resistance area product at zero bias ($R_0 \times A$) are 4×10^{-3} A/cm^2 and 21.6 Ω·cm^2, respectively. At 25K, the J_{-50mV} and R_0A are 1.9×10^{-4} A/cm^2 and 888 Ω·cm^2. The optical characteristic of the Sample A is shown in Figure 14(b), (c), and (d). The responsivity, the quantum efficiency (QE), and 50% cut-off wavelength ($\lambda_{50\%}$) are not sensitive with temperature from 30K to 77K. For 2 microns thick active layer the peak responsivity (7.5 μm) and QE is at peak responsivity at zero bias (7.5 μm) are around ~2 A/W and ~35% in the whole temperature range (Figure 14-b). The level of the QE is similar as ones reported for the InAs/GaSb SLs. The value of $\lambda_{50\%}$ changes from 9.28 μm to 9.5 μm from 30K to 77K (Figure 14-c). At 60K and below, the specific detectivity (D*) stays at the level around 4×10^{11} Jones but starts decreases as temperature increases. That is because below 60K, the dark current of the device is limited by surface leakage current, which is

insensitive with temperature. Above 60K, the dark current of the device is limited by G-R process, resulting in the decrement of D*. At 77K, the device exhibits D* of 1×10^{11} Jones.

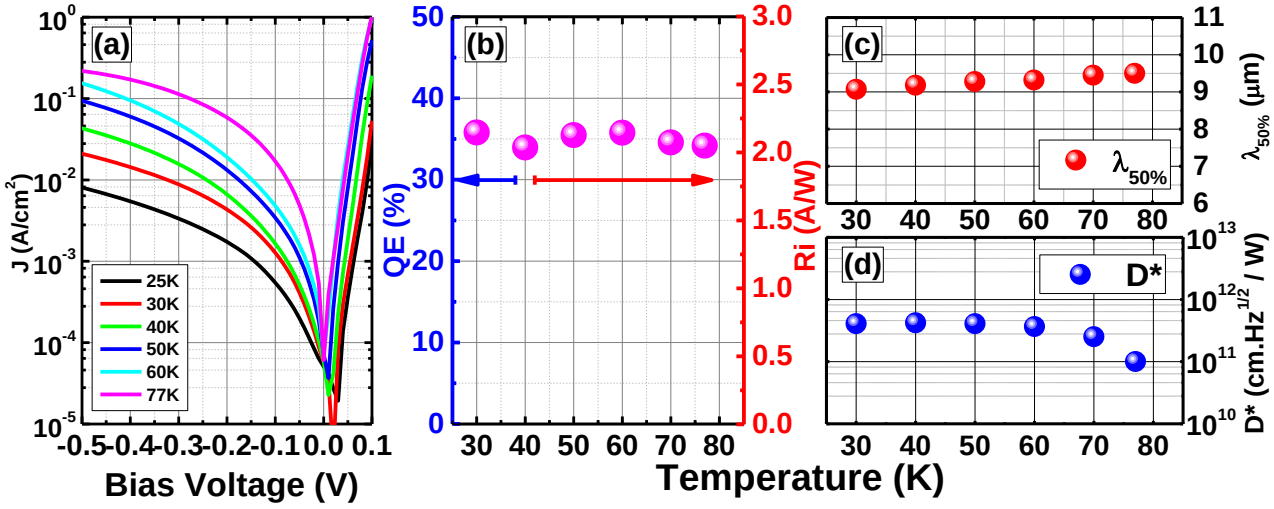

Figure 14: ***Sample A_0 temperature evolution of (a) dark current density, (b) peak responsivity (7.5 μm) and the quantum efficiency at peak responsivity, (c) 50% cut-off wavelength, and (d) specific detectivity.***

3. Conclusion

In summary, we showed that if the GaSb thickness in a InAs/GaSb superlattice is kept constant at 7 MLs, there is a residual background type change when the MLs of InAs increase from 7 to 13. When the MLs of InAs is less than 11, the T2SL exhibits p-type semiconductor behavior; when the MLs of InAs is less than 13, the T2SL exhibits n-type semiconductor behavior. The dependence of the total concentration and activation energy of 2nd kind of shallow level defect on InAs layer thickness not only provides useful information to investigate the discrepancy between the theoretical limits and the experimental performance of devices based on this material system, but also helps to further optimize the detector performance such as utilize the type of nid InAs/GaSb superlattice to avoid doping the detector.

On the other hand, intentionally undoped LWIR InAs/$InAs_{1-x}Sb_x$ T2SLs with 100% cut-off wavelength at 12 μm exhibits residually *n*-type background, with carrier concentration of 1.2×10^{16} cm^{-3} if grown at 405°C. By reducing the growth temperature to 395°C, we can reduce the *n*-type background carrier concentration to 1.6×10^{15} cm^{-3}. The *n*-type background carrier concentration can be also reduced by doping the T2SLs with Be. At the Be-doping level of 2×10^{16} cm^{-3}, the InAs/$InAs_{1-x}Sb_x$ T2SLs changes from *n*-type to *p*-type. More importantly, two different kinds of defect are observed from the evolution of the reduced carrier concentration

with temperature. Reducing the growth temperature can suppress the deep level defect by 3 times but it does not have influence on the shallow level defect.

4. **References**

[i] G. A. Sai-Halasz, R. Tsu, and L. Esaki, "A new semiconductor superlattice," Applied Physics Letters, 30(12), 651-653 (1977).

[ii] M. Razeghi, US Patent 6864552, Focal plane arrays in type II-superlattices 2005

[iii] P.-Y. Delaunay, A. Hood, B. M. Nguyen, D. Hoffman, Y. Wei, and M. Razeghi, "Passivation of type-II InAs/GaSb double heterostructure," Applied Physics Letters, 91(9), 091112-3 (2007).

[iv] C.H. Grein, J. Garland, and M.E. Flatte, *J. Electron. Mater.* **38**, 1800 (2009)

[v] G. Chen, B.-M. Nguyen, A.M. Hoang, E.K. Huang, S.R. Darvish, and M. Razeghi, *Appl. Phys. Lett.* **99**, 183503 (2011)

[vi] G. Chen, A.M. Hoang, S. Bogdanov, A. Haddadi, S.R. Darvish, and M. Razeghi, *Appl. Phys. Lett.* **103**, 223501 (2013)

[vii] G. Chen, A.M. Hoang, and M. Razeghi, *Appl. Phys. Lett.* **104**, 103509 (2014)

[viii] T. Schuler-Sandy, S. Myers, B. Klein, N. Gautum, P. Ahirwar, Z.-B. Tian, T. Rotter, G. Balakrishnan, E. Plis, and S. Krishna, *Appl. Phys. Lett.***101**, 071111 (2012)

[ix] S. Bandara, P. Maloney, N. Baril, J. Pellegrino, and M. Tidrow, *Infrared Phys. Technol.***54,** 263 (2011).

[x] D. Donetsky, S.P. Svensson, L.E. Vorobjev, and G. Belenky, *Appl. Phys. Lett.* **95** (2009).

[xi] B.C. Connelly, G.D. Metcalfe, H. Shen, and M. Wraback, *Appl. Phys. Lett.* **97** (2010).

[xii] E.H. Steenbergen, B.C. Connelly, G.D. Metcalfe, H. Shen, M. Wraback, D. Lubyshev, Y. Qiu, J.M. Fastenau, A.W.K. Liu, S. Elhamri, O.O. Cellek, and Y.-H. Zhang, *Appl. Phys. Lett.* **99** (2011).

[xiii]B.V. Olson, E.A. Shaner, J.K. Kim, J.F. Klem, S.D. Hawkins, L.M. Murray, J.P. Prineas, M.E. Flatte, and T.F. Boggess, *Appl. Phys. Lett.* **101**, 002109 (2012)

[xiv]D. Lackner, M. Steger, M.L.W. Thewalt, O.J. Pitts, Y.T. Cherng, S.P. Watkins, E. Plis, and S. Krishna, *J. Appl. Phys.* **111**, 034507 (2012)

[xv]Y. Lin, D. Wang, D. Donetsky, L. Shterengas, G. Kipshidze, G. Belenky, S.P. Svensson, W.L. Sarney, and H.S. Hier, *J. Electron Mater.* **42**(5), 918 (2013).

[xvi]K. Mahalingam, E.H. Steenbergen, G.J. Brown, and Y.-H. Zhang, *Appl. Phys. Lett.* **103**, 061908 (2013).

[xvii]E.H. Steenbergen, S. Elhamri, W.C. Mitchel, S. Mou, and G.J. Brown, *Appl. Phys. Lett.* **104**, 011104 (2014)

[xviii]G. Chen, A.M. Hoang, S. Bogdanov, A. Haddadi, P.R. Bijjam, B.-M. Nguyen, and M. Razeghi, *Appl. Phys. Lett.* **103**, 033512 (2013)

[xix] A. Hood, D. Hoffman, B.-M. Nguyen, P.-Y. Delaunay, E. Michel, and M. Razeghi, "High differential resistance type-II InAs/GaSb superlattice photodiodes for the long-wavelength infrared," Applied Physics Letters, 89(9), 093506-3 (2006)

[xx] Y. Wei and M. Razeghi, Phys. Rev. B. 69, 085316 (2004)

[xxi] S. Chaudhuri, Phys. Rev. B. 28, 4480 (1983)

[xxii] D. Hoffman, B.-M. Nguyen, P.-Y. Delaunay, A. Hood, M. Razeghi, and J. Pellegrino, "Beryllium compensation doping of InAs/GaSb infrared superlattice photodiodes," Applied Physics Letters, 91(14), 143507-3 (2007).

[xxiii]A. Hood, D. Hoffman, Y. Wei, F. Fuchs and M. Razeghi, *App. Phys. Lett.* **88**, 052112 (2006)

[xxiv]Y. Lin, D. Wang, D. Donetsky, G. Belenky, H. Hier, W.L. Sarney, and S.P. Svensson, *J. Electron. Mater.* **43** (9), 3184 (2014)